Mineralogical Magazine (2023), **87**, 568–574
doi:10.1180/mgm.2023.37

CAMBRIDGE UNIVERSITY PRESS

Article

Monazite-(Gd), a new Gd-dominant mineral of the monazite group from the Zimná Voda REE–U–Au quartz vein, Prakovce, Western Carpathians, Slovakia

Martin Ondrejka[1], Pavel Uher[1], Štefan Ferenc[2], Juraj Majzlan[3], Kilian Pollok[3], Tomáš Mikuš[4], Stanislava Milovská[4], Alexandra Molnárová[1], Radek Škoda[5], Richard Kopáčik[2], Sergii Kurylo[4] and Peter Bačík[1,6]

[1]Department of Mineralogy Petrology and Economic Geology, Faculty of Natural Sciences, Comenius University, Ilkovičova 6, Mlynská dolina, 842 15, Bratislava, Slovakia; [2]Department of Geography and Geology, Faculty of Natural Sciences, Matej Bel University, Tajovského 40, 974 01 Banská Bystrica, Slovakia; [3]Institute of Geosciences, Friedrich Schiller University, Burgweg 11, 07749 Jena, Germany; [4]Earth Science Institute, Slovak Academy of Sciences, Ďumbierska 1, 974 01, Banská Bystrica, Slovakia; [5]Department of Geological Sciences, Faculty of Science, Masaryk University, Kotlářská 2, 611 37 Brno, Czech Republic and [6]Earth Science Institute, Slovak Academy of Sciences, Dúbravská cesta 9, 840 05, Bratislava, Slovakia

Abstract

Monazite-(Gd), ideally $GdPO_4$, is a new mineral of the monazite group. It was discovered near Prakovce-Zimná Voda, ~23 km WNW of Košice, Western Carpathians, Slovakia. It forms anhedral domains (≤100 μm, mostly 10–50 μm in size), in close association with monazite-(Sm), Gd-bearing xenotime-(Y), Gd-bearing hingganite-(Y), fluorapatite and uraninite. All these minerals are hosted in a REE–U–Au quartz–muscovite vein, hosted in phyllites in an exocontact to granites. The density calculated using the average empirical formula and unit-cell parameters is 5.55 g/cm^3. The average chemical composition measured by means of electron microprobe is as follows (wt.%): P_2O_5 29.68, As_2O_5 0.15, SiO_2 0.07, ThO_2 0.01, UO_2 0.04, Y_2O_3 1.30, La_2O_3 3.19, Ce_2O_3 6.93, Pr_2O_3 1.12, Nd_2O_3 10.56, Sm_2O_3 17.36, Eu_2O_3 1.49, Gd_2O_3 22.84, Tb_2O_3 1.57, Dy_2O_3 2.27, CaO 0.21, total 99.67. The corresponding empirical formula calculated on the basis of 4 oxygen atoms is: $(Gd_{0.30}Sm_{0.24}Nd_{0.15}Ce_{0.10}La_{0.05}Dy_{0.03}Y_{0.03}Tb_{0.02}Eu_{0.02}Pr_{0.02}Ca_{0.01})_{0.98}P_{1.01}O_4$. The ideal formula is $GdPO_4$. The monazite-type structure has been confirmed by micro-Raman spectroscopy and selected-area electron diffraction. Monazite-(Gd) is monoclinic, space group $P2_1/n$, $a = 6.703(1)$ Å, $b = 6.914(1)$ Å, $c = 6.383(1)$ Å, $\beta = 103.8(1)°$, $V = 287.3(1)$ Å^3 and $Z = 4$. The middle REE enrichment of monazite-(Gd) is shared with the associated Gd-bearing xenotime-(Y) to 'xenotime-(Gd)' and Gd-bearing hingganite-(Y). This exotic REE signature and precipitation of Gd-bearing mineral assemblage is a product of selective complexing and enrichment in middle REE in low-temperature hydrothermal fluids by alteration of primary uraninite, brannerite and fluorapatite on a micro-scale. The new mineral is named as an analogue of monazite-(La), monazite-(Ce), monazite-(Nd) and monazite-(Sm) but with Gd dominant among the REE.

Keywords: monazite-(Gd); new mineral; monazite group; gadolinium; rare earth elements; Zimná Voda quartz vein; Slovakia

(Received 27 January 2023; accepted 11 May 2023; Accepted Manuscript published online: 24 May 2023; Associate Editor: Ian Terence Graham)

Introduction

Rare earth elements represent a unique set of elements having coherent behaviour and very similar properties which are responsible for their similar geochemical properties. According to the International Union for Pure and Applied Chemistry, the term rare earth elements (REE) includes lanthanoids (Ln), yttrium (Y) and scandium (Sc). However, due to the substantially smaller ionic radius of Sc^{3+} with respect to the rest of the group, Sc frequently enters different crystal-structural sites, and therefore Sc is commonly not included in the REE in geological sciences, as is the case in this work. Due to the lanthanoid contraction phenomenon, the REE are further divided, by atomic number into light (LREE: La–Nd), middle (MREE: Sm–Dy) and heavy (HREE: Ho–Lu and Y).

Minerals belonging to the monazite group are anhydrous orthophosphates (with monoclinic symmetry, space group $P2_1/n$). They contain dominant trivalent LREE cations based on their preference of the monazite-type crystal structure (Ni *et al.*, 1995). Among them, monazite-(Ce) is the most common species, whereas monazite-(La), monazite-(Nd) and monazite-(Sm) are rare, found typically in specific pegmatite, post-magmatic or sedimentary environments (e.g. Maksimović and Pantó, 1980; Graeser and Schwander, 1987; Demartin *et al.*, 1991; Pekov, 1998, 2000; Masau *et al.*, 2002; Dowman *et al.*, 2017). Despite having a generally coherent behaviour, selective REE mobilisation and

Corresponding author: Martin Ondrejka; Email: martin.ondrejka@uniba.sk
Cite this article: Ondrejka M., Uher P., Ferenc Š., Majzlan J., Pollok K., Mikuš T., Milovská S., Molnárová A., Škoda R., Kopáčik R., Kurylo S. and Bačík P. (2023) Monazite-(Gd), a new Gd-dominant mineral of the monazite group from the Zimná Voda REE–U–Au quartz vein, Prakovce, Western Carpathians, Slovakia. *Mineralogical Magazine* **87**, 568–574. https://doi.org/10.1180/mgm.2023.37

© The Author(s), 2023. Published by Cambridge University Press on behalf of The Mineralogical Society of the United Kingdom and Ireland

https://doi.org/10.1180/mgm.2023.37 Published online by Cambridge University Press

fractionation in aqueous systems is quite common and has been reported previously from different geochemical environments (e.g. Seredin, 1996; Morgan *et al.*, 2012; Göb *et al.* 2013; Lee *et al.*, 2013; Ondrejka *et al.*, 2018, 2023; Abedini *et al.*, 2019; Migdisov *et al.*, 2019; Anenburg *et al.*, 2020). In contrast to numerous LREE-dominant minerals, there is currently only one Gd-dominant mineral approved by the Commission on New Minerals, Nomenclature and Classification of the International Mineralogical Association (IMA–CNMNC, Pasero, 2023): lepersonnite-(Gd) $CaGd_2(UO_2)_{24}(SiO_4)_4(CO_3)_8(OH)_{24}{\cdot}48H_2O$, a rare REE-uranyl carbonate from the Shinkolobwe U deposit in the DR Congo (Deliens and Piret, 1982). This mineral, however, contains a relatively low absolute concentration of essential Gd (2.1 wt.% Gd_2O_3) together with minor Dy, Y and Tb.

Here, we describe a new Gd-dominant mineral monazite-(Gd), discovered in a REE–U–Au quartz vein near Prakovce, Zimná Voda, Slovakia. Monazite-(Gd) is the Gd-dominant member of the monazite group, related to monazite-(La), monazite-(Ce), monazite-(Nd) and monazite-(Sm) by substitution of Gd for other REE and having the REE composition distinctly shifted towards the MREE. The new mineral was approved in accordance with recommendations of the IMA–CNMNC (IMA2022-055; Ondrejka *et al.*, 2022) and the Levinson modifier for rare earth minerals (Levinson, 1966; Bayliss and Levinson, 1988). The symbol Mnz-Gd was given to the new mineral. The holotype specimen of monazite-(Gd) (polished thin section ZV-2A) has been deposited in the collection of the Department of Mineralogy, Petrology and Economic Geology, Faculty of Natural Sciences, Comenius University in Bratislava, Ilkovičova 6, Mlynská dolina, 84215, Bratislava, Slovak Republic under the catalogue number MMUK7660. The cotype specimen (polished thin section ZV-2A1) is deposited in the collections of the Slovak National Museum, Natural History Museum, Vajanského nábrežie 2, P.O. BOX 13, 810 06 Bratislava, Slovak Republic under the catalogue number M-20411.

Occurrence

The Zimná voda occurrence was discovered in 1975, during exploration for uranium ores (Novotný and Čížek 1979). The sample containing monazite-(Gd) was collected by Martin Ondrejka, Štefan Ferenc, Tomáš Mikuš and Alexandra Molnárová in September 2017 during reconnaissance of the Zimná Voda REE–U–Au quartz vein, Prakovce, eastern Slovakia. The site is located near the main ridge of the Slovenské Rudohorie Mts., ~5.6 km to the S of the village of Prakovce, 600 m to the NW of the Tri Studne elevation point (969 m a.s.l.) and 400 m NW of Trohánka bivouac shelter, at an altitude of ~950 m a.s.l., ca. 23 km WNW of Košice town. The geographical coordinates of the occurrence are 48.767°N and 20.913°E.

The Zimná Voda REE–U–Au vein mineralisation is located in the Lower Palaeozoic metamorphic rocks of the Bystrý Potok Formation, a part of the Gelnica Group in the Gemeric tectonic unit of the Western Carpathians, which is part of the Alpine–Carpathian Mountain belt (Bajaník *et al.* 1983; Ivanička *et al.*, 1989). Two quartz veins (Western and Eastern) containing U and Au mineralisation were found in the area. Monazite-(Gd) was found in the Western vein. The vein is located in fine-grained micaceous phyllites, with interbeds of fine-grained quartzites. It has an E–W strike, total length of ~90 m with an average dip of 65° to the S and conforms to the schistosity of the host rocks. The thickness of the vein ranges from 3 to 30 cm. Along with the contact, the rocks are intensively argillitised and locally silicified. The metamorphic rocks were intruded by Permian rare-metal granites that outcrop at a site called Hummel, ~600 m to the SW of the vein. The mineralisation probably originated by fluid-driven hydrothermal mobilisation of REE, U and Au from the surrounding metamorphic rocks induced by the intrusion of the granitic rocks (Rojkovič *et al.*, 1997; 1999). Further details and regional geology can be found in Ondrejka *et al.* (2023).

Alongside the investigated monazite-(Gd), the following minerals were identified in the Western vein: quartz, uraninite, brannerite, rutile, gold, bismuth, bismuthinite, pyrite, arsenopyrite, cobaltite, glaucodot, molybdenite, galena, tetrahedrite-(Fe), fluorapatite, monazite-(Ce), monazite-(Nd), monazite-(Sm), xenotime-(Y), hingganite-(Y), muscovite, chlorite and tourmaline; supergene minerals are represented by goethite and other undifferentiated iron oxyhydroxides, pharmacosiderite, scorodite, arseniosiderite, zeunerite, other uranyl arsenates–phosphates (most abundant are nováčekite, kahlerite, threadgoldite, rarely autunite, chistyakovaite–arsenuranospathite related mineral phases and phosphuranylite). The gadolinium-bearing mineral assemblage also includes xenotime-(Y) and hingganite-(Y) (Ondrejka *et al.*, 2023). Moreover, a Gd-dominant analogue of xenotime-(Y) is potentially the second new Gd-dominant mineral from this locality; a detailed structural study, necessary for its approval by the IMA–CNMNC, will be the subject of future investigations.

Experimental methods

The chemical composition of selected minerals was studied by a JEOL JXA-8530F electron microprobe analyser (EMPA) in wavelength-dispersive spectrometry (WDS) mode, and X-ray element mapping at the Earth Science Institute, Slovak Academy of Sciences in Banská Bystrica, Slovakia. An accelerating voltage of 15 kV and a probe current of 20 nA were used. The typical spot beam diameter varied from 2 to 8 μm; a more focused ≤1–3 μm beam was used occasionally to avoid any intermediate composition in strongly heterogeneous micro-scale areas. The determination was calibrated using natural and synthetic standards (Table 1), and raw counts were converted to wt.% of oxides using the ZAF matrix correction. Corrections of line interferences were provided using the method by Åmli and Griffin (1975). Elements with reported detection limits are given in Table 1.

Depolarised Raman measurements of monazite-(Gd) were performed on a Labram HR800 spectrometer (Horiba Jobin-Yvon), coupled with an Olympus-BX41 optical microscope. Samples were irradiated using a 532 nm frequency-doubled Nd-YAG and 633 nm He–Ne lasers. The system resolution was 2 cm^{-1}; band definition was improved using a 6-fold sub-pixel shift. Peaks were deconvoluted with a Gauss-Lorentzian function in *PeakFit*© (SeaSolve Software).

To determine the principal features of the crystal structure, we used transmission electron microscopy (TEM) on focused ion beam (FIB) lamella at the Institute of Geosciences, Friedrich Schiller University of Jena, Germany. This procedure enables measurement of electron diffraction patterns of the same phases that were analysed previously by EMP. The FIB preparation was conducted using a Quanta 3D FEG FIB-SEM instrument that enabled a progressive abrasion of the targeted area in the mineral using a focused beam of Ga ions, monitored by secondary electron (SE) and back-scattered electron (BSE) imaging. The

https://doi.org/10.1180/mgm.2023.37 Published online by Cambridge University Press

Table 1. Conditions used for the electron microprobe analyses.

Element	Line	Crystal	Standard	Detection limit (3σ) in ppm
S	*Kα*	PETL	baryte	60–80
P	*Kα*	PETL	apatite	135–160
As	*Lα*	TAP	GaAs	210–255
Si	*Kα*	TAP	albite	90–100
Th	*Mα*	PETL	thorianite	130–135
U	*Mβ*	PETL	UO_2	195–205
Al	*Kα*	TAP	albite	65–70
Y	*Lα*	PETL	YPO_4	160–180
La	*Lα*	LIFH	$LaPO_4$	280–305
Ce	*Lα*	LIFH	$CePO_4$	250–275
Pr	*Lβ*	LIFH	$PrPO_4$	480–505
Nd	*Lα*	LIFH	$NdPO_4$	260–275
Sm	*Lβ*	LIFH	$SmPO_4$	550–590
Eu	*Lα*	LIFH	$EuPO_4$	270–285
Gd	*Lβ*	LIFH	$GdPO_4$	575–610
Tb	*Lα*	LIFH	$TbPO_4$	310–360
Dy	*Lα*	LIFH	$DyPO_4$	315–355
Ho	*Lβ*	LIFH	$HoPO_4$	685–720
Er	*Lα*	LIFH	$ErPO_4$	330–360
Tm	*Lα*	LIFH	$TmPO_4$	300–380
Yb	*Lα*	LIFH	$YbPO_4$	360–385
Lu	*Lα*	LIFH	$LuPO_4$	390–405
Ca	*Kα*	PETL	apatite	45–50
Sr	*Lα*	TAP	celestine	95–195
Fe	*Kα*	LIF	hematite	260–295
Mn	*Kα*	LIF	rhodonite	265–290
Pb	*Mα*	PETL	$PbCO_3$	140–160

monazite-(Gd) lamella was prepared by FIB as a TEM foil on a copper FIB lift-out grid. Selected-area electron diffraction (SAED) patterns of monazite-(Gd) were taken at 13 zone axis orientations on a single crystal.

Element contents in the mineral formula are expressed in atoms per formula unit (apfu), the monazite formula was normalised to 4 oxygen atoms.

Appearance and physical properties

Monazite-(Gd) forms anhedral domains (≤100 μm in size, mostly 10–50 μm), usually as intergrowths with other crystals or aggregates of monazite-(Sm) and Gd-bearing xenotime-(Y) (≤150 μm in size), fluorapatite, Gd-bearing hingganite-(Y) and uraninite scattered in quartz–muscovite gangue (Fig. 1). Among four monazite-group species recognised in the Western vein at Zimná Voda, monazite-(Ce) is the most common and is the only LREE phosphate which occurs in all of the six samples studied. Monazite-(Nd), monazite-(Sm) and monazite-(Gd) were found only in the ZV-2 sample, though in multiple thin sections. The lustre, hardness, cleavage and parting of monazite-(Gd) could not be determined, nor could density be measured due to an insufficient quantity for physical measurement. The density of 5.55 g/cm^3 was calculated on the basis of average empirical formula and calculated unit-cell volume (see below). The density of the ideal formula $GdPO_4$ is 5.99 g cm^{-3}.

Chemical composition

Chemical analyses were carried-out on crystals of the holotype specimen (ZV-2A thin section) and further crystals of the cotype specimen (ZV-2A1) and the composition is shown in Table 2. The individual crystals are chemically homogeneous, with no distinct variations in the core–rim profile. Locally, there may be a heterogeneous composition reflecting irregular μm-scale domains of different REE distributions. The crystals analysed have a composition with Gd>Sm>Nd>Ce>La (20.1–23.4 wt.% Gd_2O_3, 0.25–0.31 apfu Gd; 16.2–18.3 wt.% Sm_2O_3, 0.21–0.25 apfu Sm, 9.8–11.6 wt.% Nd_2O_3, 0.13–0.17 apfu Nd, 6.6–8.6 wt.% Ce_2O_3, 0.10–0.13 apfu Ce, 3.0–4.3 wt.% La_2O_3, 0.05–0.06 apfu La). The average chemical composition of monazite-(Gd) calculated from six point electron-microprobe analyses is as follows (wt.%): P_2O_5 29.68, As_2O_5 0.15, SiO_2 0.07, ThO_2 0.01, UO_2 0.04, Y_2O_3 1.30, La_2O_3 3.19, Ce_2O_3 6.93, Pr_2O_3 1.12, Nd_2O_3 10.56, Sm_2O_3 17.36, Eu_2O_3 1.49, Gd_2O_3 22.84, Tb_2O_3 1.57, Dy_2O_3 2.27, Ho_2O_3 0.24, Er_2O_3 0.20, Tm_2O_3 0.02, Yb_2O_3 0.28, Lu_2O_3 0.01, FeO 0.08, MnO 0.03, CaO 0.21, PbO 0.01, Cl 0.03, total 99.67. The corresponding empirical formula calculated on the basis of 4 oxygen atoms is: $(Gd_{0.30}Sm_{0.24}Nd_{0.15}Ce_{0.10}La_{0.05}Dy_{0.03}Y_{0.03}Tb_{0.02}Eu_{0.02}Pr_{0.02}Ca_{0.01})_{0.98}P_{1.01}O_4$ which leads to the end-member formula $GdPO_4$ requiring 71.86 Gd_2O_3, 28.14 P_2O_5 and total 100 wt.%.

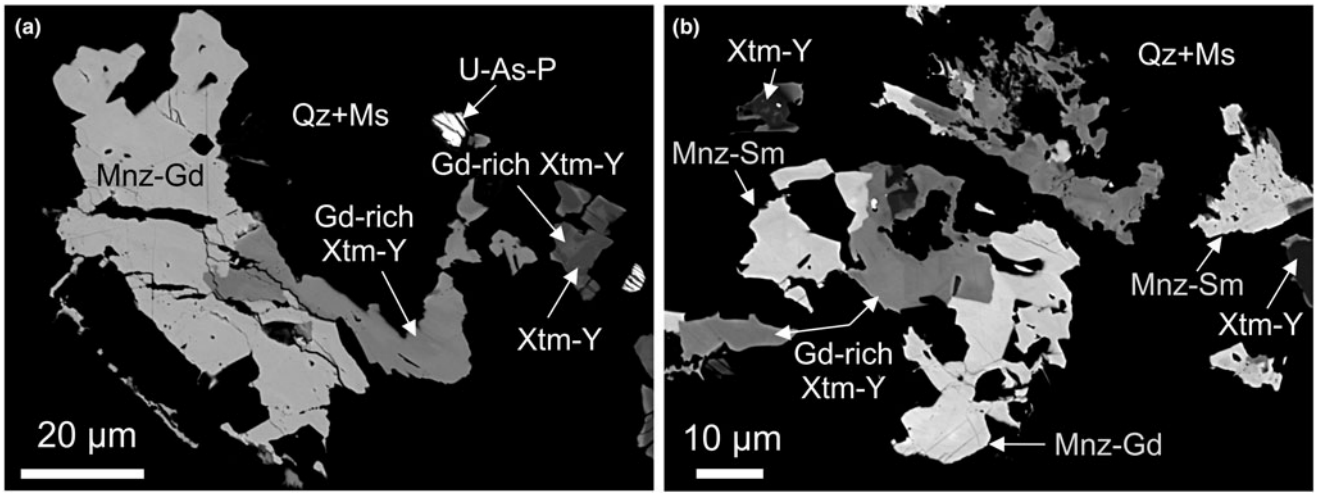

Figure 1. Back-scattered electron images of (a) large aggregate of monazite-(Gd) (Mnz-Gd) with xenotime-(Y) (Xtm-Y), Gd-bearing xenotime-(Y) (Gd-rich Xtm-Y) and uranyl arsenates–phosphates (U–As–P) in quartz–muscovite gangue (Qz + Ms). (b) Monazite-(Gd) (Mnz-Gd) and monazite-(Sm) (Mnz-Sm) with xenotime-(Y) (Xtm-Y) and Gd-bearing xenotime-(Y) (Gd-rich Xtm-Y) in quartz–muscovite gangue (Qz + Ms). (a) Holotype specimen, polished thin section ZV-2A; (b) cotype specimen: ZV-2A1; symbols from Warr (2021).

https://doi.org/10.1180/mgm.2023.37 Published online by Cambridge University Press

Table 2. Representative and average electron microprobe analyses and mineral formula of monazite-(Gd).

Wt.%	1	2	3	4	5	6	Mean ($n = 6$)	apfu	1	2	3	4	5	6	Mean ($n = 6$)
SO_3	–	0.01	–	–	–	–	–	S^{6+}	0.000	0.000	0.000	0.000	0.000	0.000	0.000
P_2O_5	29.46	30.12	29.21	29.49	29.98	29.82	29.68	P^{5+}	1.005	1.013	0.999	1.008	1.006	1.012	1.007
As_2O_5	0.07	0.15	0.22	0.11	0.23	0.14	0.15	As^{5+}	0.001	0.003	0.005	0.002	0.005	0.003	0.003
SiO_2	0.03	0.06	0.12	0.04	0.17	0.02	0.07	Si^{4+}	0.001	0.002	0.005	0.002	0.007	0.001	0.003
ThO_2	–	0.01	0.04	0.00	0.02	–	0.01	ΣA	1.008	1.019	1.009	1.012	1.017	1.015	1.013
UO_2	0.06	0.00	–	0.04	–	0.11	0.04	Th^{4+}	0.000	0.000	0.000	0.000	0.000	0.000	0.000
Al_2O_3	0.02	–	–	–	–	–	–	U^{4+}	0.001	0.000	0.000	0.000	0.000	0.001	0.000
Y_2O_3	1.23	1.29	1.39	1.10	1.48	1.29	1.30	Al^{3+}	0.001	0.000	0.000	0.000	0.000	0.000	0.000
La_2O_3	3.01	3.06	3.22	3.38	3.28	3.16	3.19	Y^{3+}	0.026	0.027	0.030	0.024	0.031	0.028	0.028
Ce_2O_3	6.88	7.28	7.14	6.95	6.73	6.58	6.93	La^{3+}	0.045	0.045	0.048	0.050	0.048	0.047	0.047
Pr_2O_3	1.11	1.10	1.24	1.09	1.15	1.04	1.12	Ce^{3+}	0.102	0.106	0.106	0.103	0.098	0.097	0.102
Nd_2O_3	10.62	10.89	10.73	10.53	9.76	10.84	10.56	Pr^{3+}	0.016	0.016	0.018	0.016	0.017	0.015	0.016
Sm_2O_3	17.45	17.30	17.61	16.70	17.68	17.40	17.36	Nd^{3+}	0.153	0.155	0.155	0.152	0.138	0.155	0.151
Eu_2O_3	1.62	1.50	1.26	1.58	1.59	1.41	1.49	Sm^{3+}	0.242	0.237	0.245	0.232	0.241	0.240	0.240
Gd_2O_3	23.36	22.49	22.31	23.33	22.74	22.83	22.84	Eu^{3+}	0.022	0.020	0.017	0.022	0.021	0.019	0.020
Tb_2O_3	1.58	1.59	1.62	1.58	1.50	1.55	1.57	Gd^{3+}	0.312	0.296	0.299	0.312	0.299	0.303	0.304
Dy_2O_3	2.31	2.02	2.22	2.34	2.49	2.22	2.27	Tb^{3+}	0.021	0.021	0.022	0.021	0.020	0.020	0.021
Ho_2O_3	0.20	0.23	0.20	0.27	0.24	0.31	0.24	Dy^{3+}	0.030	0.026	0.029	0.030	0.032	0.029	0.029
Er_2O_3	0.10	0.31	0.17	0.16	0.27	0.20	0.20	Ho^{3+}	0.003	0.003	0.003	0.003	0.003	0.004	0.003
Tm_2O_3	0.01	0.02	0.01	0.01	0.02	0.04	0.02	Er^{3+}	0.001	0.004	0.002	0.002	0.003	0.003	0.003
Yb_2O_3	0.35	0.14	0.31	0.32	0.23	0.31	0.28	Tm^{3+}	0.000	0.000	0.000	0.000	0.000	0.000	0.000
Lu_2O_3	0.02	–	–	0.01	0.01	–	0.01	Yb^{3+}	0.004	0.002	0.004	0.004	0.003	0.004	0.003
FeO_t	0.03	0.12	0.08	0.04	0.16	0.06	0.08	Lu^{3+}	0.000	0.000	0.000	0.000	0.000	0.000	0.000
MnO	0.04	0.03	–	0.03	–	0.05	0.03	Fe^{2+}	0.001	0.004	0.003	0.001	0.005	0.002	0.003
CaO	0.10	0.21	0.18	0.14	0.49	0.12	0.21	Mn^{2+}	0.001	0.001	0.000	0.001	0.000	0.002	0.001
PbO	–	–	0.05	–	0.03	–	0.01	Ca^{2+}	0.004	0.009	0.008	0.006	0.021	0.005	0.009
Cl	0.04	0.03	0.03	0.03	0.02	0.05	0.03	Pb^{2+}	0.000	0.000	0.001	0.000	0.000	0.000	0.000
O=Cl	–0.01	–0.01	–0.01	–0.01	–0.01	–0.01	–0.01	ΣB	0.986	0.971	0.989	0.981	0.981	0.974	0.980
Total	99.68	99.94	99.35	99.25	100.27	99.55	99.67	ΣAB	1.994	1.990	1.998	1.993	1.998	1.989	1.994

– not detected

In general, the element distribution shows enrichment towards the MREE, depletion of LREE and negligible HREE (Ho–Lu)+Y abundances. The chondrite-normalised patterns exhibit conspicuous maxima at Sm and Gd (MREE hump) and a distinct downward concave W-type tetrad effect on the first tetrad (La–Nd) (for further details, see Ondrejka *et al.*, 2023). Concentrations of Th and U were usually below the detection limit of the EPMA; Th rarely attains 1.1 wt.% ThO_2 (0.01 apfu Th) in measurements having also increased Si content (≤0.7 wt.% SiO_2, 0.03 apfu Si). These analyses attest to limited $ThSiREE_{-1}P_{-1}$ huttonite substitution. Satisfactory analytical totals (98–100 wt.%) and stoichiometry calculated on an anhydrous basis indicate that any potential role of a tetrahedral array of $(OH)^-$ groups is negligible. Other trace elements (Ca, Sr, Fe, Pb, S and As) have negligible concentrations or are below detection limits.

Crystallography

Monazite-(Gd) is isostructural with other monazite-group minerals; its monoclinic (space group $P2_1/n$) structure consists of isolated PO_4 tetrahedra interconnected by $(REE)O_9$ polyhedra (Ni *et al.*, 1995). A larger REE-containing polyhedron in monazite with the coordination of 9 compared to xenotime with the coordination of 8 allows the incorporation of larger cations; therefore, the monazite structure prefers LREE (Miyawaki and Nakai, 1993). Consequently, monazite crystals with MREE enrichment are rare.

Single-crystal X-ray diffraction studies of monazite-(Gd) were not carried-out due to the small size of the crystals. However, the monazite structure is well known; therefore, selected-area electron diffraction (SAED) patterns were used to confirm the unit-cell dimensions and the symmetry of monazite-(Gd) (Fig. 2). Scanning transmission electron microscope (STEM) images at low magnification and high camera length (LMSTEM) were used to image the entire TEM-lamella. It consists of a large single crystal with sub-grains which are cross-cut by a veinlet. The neighbouring or included mineral is chlorite. The STEM images at low camera length (HAADF images) show contrast which is sensitive to the mean atomic number. These STEM images confirm the homogeneity of the sample. Slight contrast occurs at sub-grain boundaries, probably due to slight density changes there. Other changes in contrast can be correlated to thickness differences of the lamella which is an artefact from the FIB preparation.

Selected-area electron diffraction (SAED) on various zone axes resulted in 45 unique reflections that allowed for a reasonable refinement of the lattice parameters (Table 3). Note that the values are less precise than those extracted from X-ray diffraction data because the θ angles in electron diffraction are extremely small. The limited number of reflections from only a part of the reciprocal space leads to a relatively large error – larger for c because the c axis is at a high angle to the FIB sample. Thus, the reflections from (001) could not be observed. The unit-cell parameters were calculated with the *UnitCell* program (Holland and Redfern, 1997) as $a = 6.71(2)$ Å, $b = 6.98(2)$ Å, $c = 6.55(5)$ Å, $\beta = 104.4(6)°$, $V = 297.1(4)$ Å^3 and $Z = 4$.

The monazite structure is relatively simple; therefore, there is a near-ideal linear trend of decreasing unit-cell parameters with decreasing ionic radii of REE cations in synthetic $REEPO_4$ with a monazite structure (Ni *et al.*, 1995; Ushakov *et al.*, 2001). In contrast, the β angle has an inverse near-linear correlation with the REE ionic radii, it increases with smaller radii (Ni *et al.*, 1995). Consequently, it is possible to assume that the unit-cell parameters of the observed mineral probably correspond to the weighted average of the corresponding end-member unit-cell parameters. This assumption allowed the calculation of unit-cell parameters

https://doi.org/10.1180/mgm.2023.37 Published online by Cambridge University Press

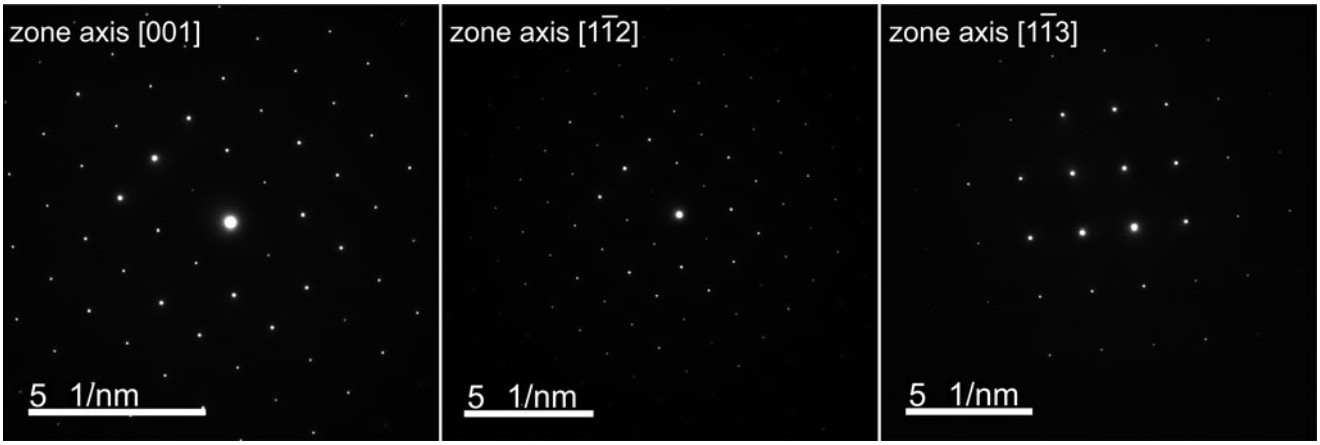

Figure 2. Electron diffraction patterns of the monazite-(Gd) crystal along the zone axes specified in each panel.

Table 3. Unit-cell parameters for natural monazite members and synthetic monazite $REEPO_4$ compounds.

	a (Å)	*b* (Å)	*c* (Å)	β (°)	*V* (Å^3)	Reference
Monazite-(Ce)	6.790(1)	7.020(1)	6.467(1)	103.4(1)	299.9(1)	Ni *et al.* (1995)
Monazite-(Nd)	6.745(4)	6.964(4)	6.435(4)	103.7(1)	293.7(2)	Graeser and Schwander (1987)
Monazite-(Sm)	6.725(1)	6.936(1)	6.448(1)	104.0(1)	291.8(1)	Masau *et al.* (2002)
Monazite-(Gd)	6.703(1)	6.914(1)	6.383(1)	103.8(1)	287.3(1)	This work
$LaPO_4$	6.8242(6)	7.0792(5)	6.4919(6)	103.0(1)	305.6(1)	Ushakov *et al.* (2001)
$CePO_4$	6.7971(4)	7.0262(3)	6.4736(4)	103.5(1)	300.6(1)	Ushakov *et al.* (2001)
$PrPO_4$	6.7687(5)	6.9900(3)	6.4439(4)	103.5(1)	296.5(1)	Ushakov *et al.* (2001)
$NdPO_4$	6.7392(9)	6.9621(6)	6.4053(6)	103.6(1)	292.1(1)	Ushakov *et al.* (2001)
$SmPO_4$	6.6891(3)	6.8958(3)	6.3770(6)	103.9(1)	285.5(1)	Ushakov *et al.* (2001)
$EuPO_4$	6.6660(7)	6.8684(6)	6.3486(8)	103.9(1)	282.2(1)	Ushakov *et al.* (2001)
$GdPO_4$	6.6511(1)	6.8471(1)	6.3343(1)	104.0(1)	279.9(1)	Ushakov *et al.* (2001)
$TbPO_4$	6.611(1)	6.813(2)	6.314(1)	104.1(2)	275.8(2)	Ushakov *et al.* (2001)

from the weighted sum of end-members as $a = 6.703(1)$ Å, $b = 6.914(1)$ Å, $c = 6.383(1)$ Å, $\beta = 103.8(1)°$, $V = 287.3(1)$ Å^3 and $Z = 4$. These are, in general, lower than unit-cell parameters calculated from SAED. The difference can be attributed to the variations in REE, which, although not significant, is observable. This suggests that the average composition from which the unit-cell size was calculated could be slightly different to the composition of crystal fragments from which SAED patterns were measured. Moreover, the accuracy of the unit-cell parameters is limited by relatively large errors in SAED measurements, as explained above. For comparison, unit-cell parameters for natural monazite members and synthetic monazite $REEPO_4$ compounds are presented in Table 3.

Raman spectroscopy

The Raman spectrum of monazite-(Gd) has already been published in supplementary material to Ondrejka *et al.* (2023) and is in good agreement with other monazite-group mineral species. All the Raman bands of the monazite-(Gd) occur in the range of up to 1200 cm^{-1} (Table 4). Two groups of lines were observed: from 100 to 700 cm^{-1}, with dominant bands at 423 cm^{-1} and 472 cm^{-1} and 950–1100 cm^{-1}, with the most intensive bands centred at 981 cm^{-1} and having an asymmetric shape.

A Raman spectrum of monazite is predicted to contain 36 ($18A_g + 18B_g$) modes (Begun *et al.*, 1981; Ruschel *et al.*, 2012; Heuser *et al.*, 2014). The bands below 700 cm^{-1} correspond to lattice vibrations, translations and rotations, the *A*-PO_4 movements and symmetric bending (ν_2), and asymmetric bending (ν_4) vibrations of the PO_4 tetrahedra. The symmetric (ν_1) and

Table 4. Raman bands for monazite-(Gd)

Band (cm^{-1})	Symmetry	Assignment
401	B_g	Lattice
423	A_g	Lattice
426	A_g	Lattice
471	A_g	$\nu_2[PO_4]$
472	A_g	$\nu_2[PO_4]$
538	A_g	$\nu_2[PO_4]$
549	A_g	$\nu_2[PO_4]$
562	A_g	$\nu_2[PO_4]$
573	A_g	$\nu_2[PO_4]$
576	A_g	$\nu_2[PO_4]$
595	B_g	$\nu_2[PO_4]$
614	A_g	$\nu_2[PO_4]$
626	A_g	$\nu_4[PO_4]$
629	A_g	$\nu_4[PO_4]$
636	A_g	$\nu_4[PO_4]$
956	A_g	$\nu_1[PO_4]$
977	A_g	$\nu_1[PO_4]$
981	A_g	$\nu_1[PO_4]$
982	A_g	$\nu_1[PO_4]$
997	A_g	$\nu_1[PO_4]$
1035	B_g	$\nu_1[PO_4]$
1065	A_g	$\nu_3[PO_4]$
1082	B_g	$\nu_3[PO_4]$

https://doi.org/10.1180/mgm.2023.37 Published online by Cambridge University Press

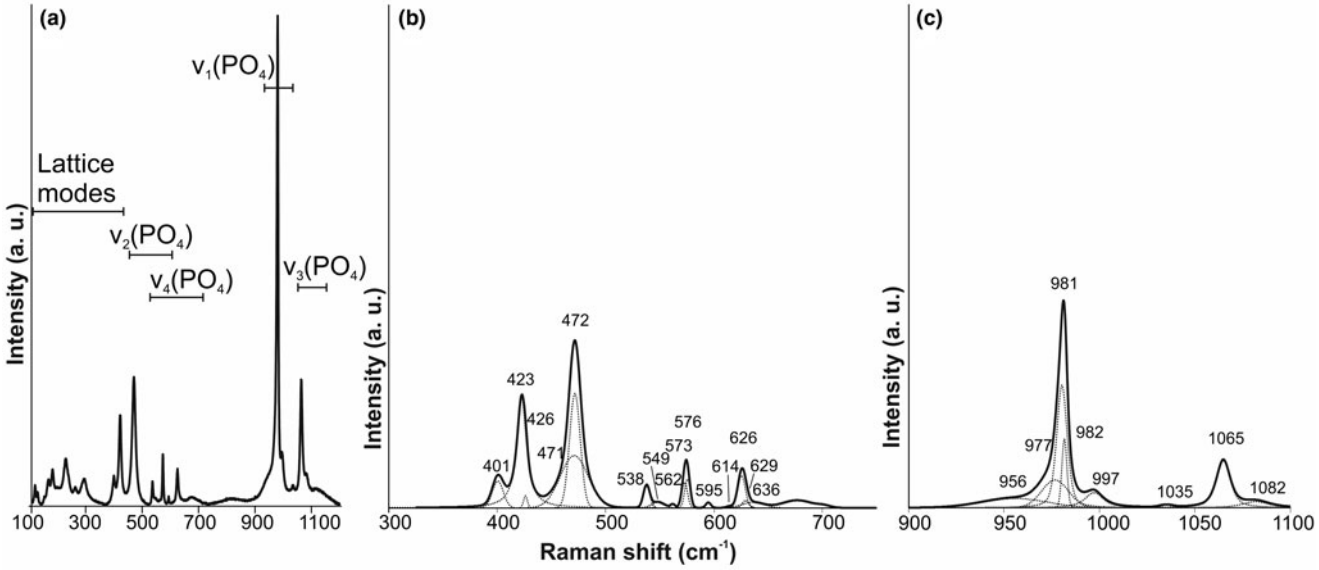

Figure 3. Depolarised 532 nm-excited Raman spectrum of monazite-(Gd) with its peak wavenumbers. (a) Full range spectrum with assigned Raman bands. (b and c) Deconvolution of spectrum to single Gaussian–Lorentzian-shaped bands in the regions of 300–750 cm^{-1} and 900–1100 cm^{-1}. Intensity scale bar in arbitrary units (a.u.).

antisymmetric stretching (ν_3) vibrations region of the PO_4-tetrahedra is expressed in the 900–1100 cm^{-1} region (Fig. 3), where ν_1 are the most intensive.

Discussion

Monazite-(Gd) is a new lanthanoid orthophosphate mineral of the monazite group with a unique Gd-dominance over the other REE cations. It represents only the second Gd-dominant mineral, described in nature, and approved by IMA–CNMNC, after lepersonnite-(Gd), $CaGd_2(UO_2)_{24}(SiO_4)_4(CO_3)_8(OH)_{24}{\cdot}48H_2O$, from the Shinkolobwe uranium deposit, DR Congo (Deliens and Piret, 1982). However, monazite-(Gd) contains a significantly higher content of Gd: 20.1–23.4 wt.% Gd_2O_3 than lepersonnite-(Gd) (only 2.1 wt.% Gd_2O_3, Deliens and Piret, 1982). Beside monazite-(Gd), monazite-(Ce), monazite-(Nd) and monazite-(Sm) from the Zimná Voda quartz vein are also enriched in Gd (2.5 to 19.1 wt.% Gd_2O_3, 0.03 to 0.25 apfu Gd; Ondrejka *et al.*, 2023). Moreover, rare occurrences of MREE (Nd, Sm and Gd)-rich compositions in the monazite-group minerals have been described from some magmatic rocks. Monazite-(Sm) from the Annie Claim #3 pegmatite, Canada had 12.1−13.5 wt.% Gd_2O_3 (0.16−0.18 apfu Gd; Masau *et al.*, 2002). Monazite-(Ce) to -(Sm) with 4.7−8.9 wt.% Gd_2O_3 (0.06−0.12 apfu Gd) was detected in the Utsumine and Siohira granites and Shimo-ono pegmatite, Japan (Hoshino *et al.*, 2012). There was 5.7−7.5 wt.% Gd_2O_3 (0.07−0.10 apfu Gd) in monazite-(Nd) from Sierra de Cobres carbonatite dykes, Argentina (Del Blanco *et al.*, 1998) and 2.9−4.8 wt.% Gd_2O_3 in monazite-(Ce) to monazite-(Nd) from the Abu Rusheid lamprophyre dyke, Egypt (Ali, 2012). Lesser Gd enrichment of up to 3.25 wt.% Gd_2O_3 (≤0.04 apfu Gd) has also been detected in skeletal monazite-(Ce) from the Oldřich pegmatite vein, Dolní Bory, Czech Republic (Výravský, 2014) and 2.2 to 2.8 wt.% Gd_2O_3 (0.03−0.04 apfu Gd) in low-temperature, authigenic monazite-(Nd) and monazite-(La) from bauxite deposits at Marmara, Greece and Liverovici, Montenegro (Maksimović and Pantó, 1980, 1996).

Such unusual enrichment of MREE (Gd, Nd and Sm) in monazite-group members as well as in some other REE minerals [e.g. xenotime-(Y) and hingganite-(Y)] could be a result of selective complexing of REE during granite to pegmatite sequence solidification in aqueous F–Li–CO_2-bearing fluids (Masau *et al.*, 2002). Moreover, late-hydrothermal alteration of MREE-enriched precursors (uraninite, brannerite and fluorapatite) is considered as the principal factor for precipitation of monazite-(Gd) and associated Gd-rich minerals (Ondrejka *et al.*, 2023).

Acknowledgements. This work was supported by the Slovak Research and Development Agency under the contracts APVV-18-0065, APVV-19-0065, VEGA 1/0467/20, VEGA 1/0563/22 and by OP VVV project (Geobarr CZ.02.1.01/0.0/0.0/16_026/0008459 to R.S.). K.P. thanks F. Langenhorst for support and access to the FIB-SEM and TEM facilities in Jena, which are funded by the DFG via grant LA830/14-1. We thank Ľubomír Orovčík (Institute of Materials and Machine Mechanics, Slovak Academy of Sciences) for his attempt with the EBSD technique. Finally, we thank Peter Leverett, two anonymous reviewers, Ian Graham (Associate Editor) and Stuart Mills (Principal Editor) for their constructive suggestions.

Competing interests. The authors declare none.

References

Abedini A., Rayaei Azizi M. and Calagari A.A. (2019) REE tetrad effect as a powerful indicator of formation conditions of karst bauxites: a case study of the Shahindezh Deposit, NW Iran. *Acta Geologica Sinica*, **93**, 912–927.

Ali M.A. (2012) Mineral chemistry of monazite-(Nd), xenotime-(Y), apatite, fluorite and zircon hosting in lamprophyre dyke in Abu Rusheid area, South Eastern Desert, Egypt. *Geologija*, **55**, 93–106.

Åmli R. and Griffin W.L. (1975) Microprobe analysis of REE minerals using empirical correction factors. *American Mineralogist*, **60**, 599–606.

Anenburg M. (2020) Rare earth mineral diversity controlled by REE pattern shapes. *Mineralogical Magazine*, **84**, 629–639.

Bajaník Š., Hanzel V., Mello J., Pristaš J., Reichwalder P., Snopko L., Vozár J. and Vozárová A. (1983) *Explanation to geological map of the Slovenské Rudohorie Mts. – Eastern part, 1:50 000*. State Geological Institute of D. Štúr, Bratislava, 223 pp. [in Slovak].

Bayliss P. and Levinson A.A. (1988) A system of nomenclature for rare-earth mineral species: Revision and extension. *American Mineralogist*, **73**, 422–423.

https://doi.org/10.1180/mgm.2023.37 Published online by Cambridge University Press

Begun G.M., Beall G.W., Boatner L.A., and Gregor W.J. (1981) Raman spectra of the rare earth orthophosphates. *Journal of Raman Spectroscopy*, **11**, 273–278.

Del Blanco M., Ulbrich M.C., Echeveste H. and Vlach S.R.F. (1998) Las monacitas-(Nd) con samario de Los Diques carbontíticos del sector nororiental de la Sierra de Cobres, Slata, Argentina. *IV Reunion de Mineralogia y Metalogenia Universidad Nacional der Sur – Bahía Blanca. MINMER'98-EDIUNS*, 63–69 [in Spanish].

Deliens M. and Piret P. (1982) Bijvoetite et lepersonnite carbonates hydratés d'uranyle et des terres rares de Shinkolobwe, Zaïre. *The Canadian Mineralogist*, **20**, 231–238 [in French].

Demartin F., Pilati T., Diella V., Donzelli S. and Gramaccioli C.M. (1991) Alpine monazite: further data. *The Canadian Mineralogist*, **29**, 61–67.

Dowman E., Wall F., Treloar P.J. and Rankin A.H. (2017) Rare-earth mobility as a result of multiple phases of fluid activity in fenite around the Chilwa Island Carbonatite, Malawi. *Mineralogical Magazine*, **81**, 1367–1395.

Göb S., Gühring J-E, Bau M. and Markl G. (2013) Remobilization of U and REE and the formation of secondary minerals in oxidized U deposits. *American Mineralogist*, **98**, 530–548.

Graeser S. and Schwander H. (1987) Gasparite-(Ce) and monazite-(Nd): two new minerals to the monazite group from the Alps. *Schweizerische Mineralogische und Petrographische Mitteilungen*, **67**, 103–113.

Heuser J., Bukaemskiy A.A., Neumeier S., Neumann A. and Bosbach D. (2014) Raman and infrared spectroscopy of monazite-type ceramics used for nuclear waste conditioning. *Progress in Nuclear Energy*, **72**, 149–155.

Holland T.J.B. and Redfern S.A.T. (1997) Unit cell refinement from powder diffraction data; the use of regression diagnostics. *Mineralogical Magazine*, **61**, 65–77.

Hoshino M., Watanabe Y. and Ishihara S. (2012) Crystal chemistry of monazite from the granitic rocks of Japan: petrogenetic implications. *The Canadian Mineralogist*, **50**, 1331–1346.

Ivanička J., Snopko L., Snopková P. and Vozárová A. (1989) Gelnica group–Lower unit of Spišsko-Gemerské Rudohorie Mts. (West Carpathians), Early Paleozoic. *Geologica Carpathica*, **40**, 483–501.

Lee S.G., Asahara Y., Tanaka T., Lee S.R. and Lee T. (2013) Geochemical significance of the Rb-Sr, La-Ce and Sm-Nd isotope systems in A-type rocks with REE tetrad patterns and negative Eu and Ce anomalies: The Cretaceous Muamsa and Weolaksan granites, South Korea. *Chemie der Erde*, **73**, 75–88.

Levinson A.A. (1966) A system of nomenclature for rare-earth minerals. *American Mineralogist*, **51**, 152–158.

Maksimović Z. and Pantó G. (1980) Bastnäsite-(La) and monazite-(Nd), a new variety of monazite, from the Marmara bauxite deposit (Greece). *Bulletin Tome LXXII: Classe des Sciences Naturelles et Mathematiques*, **20**, 35–42.

Maksimović Z.J and Pantó G. (1996) Authigenic rare earth minerals in karst-bauxites and karstic nickel deposits. Pp. 257–279. in *Rare Earth Minerals* (P. Jones, F. Wall and C.T. Williams, editors). The Mineralogical Society Series, **7**. Chapman & Hall, London.

Masau M., Černý P., Cooper M.A., Chapman R. and Grice J.D. (2002) Monazite-(Sm), a new member of the monazite group from the Annie Claim #3 granitic pegmatite, Southeastern Manitoba. *The Canadian Mineralogist*, **40**, 1649–1655.

Migdisov A., Guo X., Nisbet H., Xu H. and Williams-Jones A.E. (2019) Fractionation of REE, U, and Th in natural ore-forming hydrothermal systems: Thermodynamic modeling. *Journal of Chemical Thermodynamics*, **128**, 305–319.

Miyawaki R. and Nakai I. (1993) Crystal structures of rare earth minerals. Pp. 249–518 in: *Handbook on the Physics and Chemistry of Rare Earths*, Vol.16., Chapter 108 (Gschneidner K. A. Jr. and Eyring L., editors). Elsevier Science Publishers B.V., Amsterdam.

Morgan B., Rate A.W., Burton E.D. and Smirk M.N. (2012) Enrichment and fractionation of rare earth elements in FeS- and organic-rich estuarine sediments receiving acid sulfate soil drainage. *Chemical Geology*, **308–309**, 60–73.

Ni Y., Hughes J.M. and Mariano A.N. (1995) Crystal chemistry of the monazite and xenotime structures. *American Mineralogist*, **80**, 21–26.

Novotný L. and Čížek P. (1979) New occurrence of uranium and gold, southern from Prakovce in Spišsko-gemerské Rudohorie Mts. *Mineralia Slovaca*, **11**, 188–190 [In Slovak].

Ondrejka M., Bačík P., Sobocký T., Uher P., Škoda R., Mikuš T., Luptáková J. and Konečný P. (2018) Minerals of the rhabdophane group and the alunite supergroup in microgranite: products of low temperature alteration in a highly acidic environment from the Velence Hills, Hungary. *Mineralogical Magazine*, **82**, 1277–1300.

Ondrejka M., Uher P., Ferenc Š., Majzlan J., Pollok K., Milovská S., Mikuš T., Molnárová A., Škoda R., Kopáčik R., Orovčík L. and Bačík P. (2022) Monazite-(Gd), IMA 2022-055, in: CNMNC Newsletter 70. *Mineralogical Magazine*, **87**, 160–168, https://doi.org/10.1180/mgm.2022.135

Ondrejka M., Uher P., Ferenc Š., Milovská S., Mikuš T., Molnárová A., Škoda R., Kopáčik R. and Bačík P. (2023) Gadolinium-dominant monazite and xenotime: selective hydrothermal enrichment of middle REE during low-temperature alteration of uraninite, brannerite and fluorapatite (the Zimná Voda REE-U-Au quartz vein, Western Carpathians, Slovakia), *American Mineralogist*, **108**, 754–768.

Pasero M. (2023) *The New IMA List of Minerals*. International Mineralogical Association. Commission on new minerals, nomenclature and classification (IMA-CNMNC). http://cnmnc.units.it/

Pekov I.V. (1998) *Minerals First Discovered on the Territory of the Former Soviet Union*. Ocean Pictures Ltd, Moscow, 369 pp.

Pekov I.V. (2000) *Lovozero Massif*. Ocean Pictures Ltd., Moscow, 480 pp.

Rojkovič I., Háber M. and Novotný L. (1997) U-Au-Co-Bi-REE mineralization in the Gemeric unit (Western Carpathians, Slovakia). *Geologica Carpathica*, **48**, 303–313.

Rojkovič I., Konečný P., Novotný L., Puškelová Ľ. and Streško V. (1999) Quartz-apatite-REE vein mineralization in Early Paleozoic rocks of the Gemeric Superunit, Slovakia. *Geologica Carpathica*, **50**, 215–227.

Ruschel K., Nasdala L., Kronz A., Hanchar J.M., Többens D.M., Škoda R., Finger F. and Möller A. (2012) A Raman spectroscopic study on the structural disorder of monazite–(Ce). *Mineralogy and Petrology*, **105**, 41–55.

Seredin V.V. (1996) Rare earth element-bearing coals from the Russian Far East deposits. *International Journal of Coal Geology*, **30**, 101–129.

Ushakov S.V., Helean K.B., Navrotsky A. and Boatner L.A. (2001) Thermochemistry of rare-earth orthophosphates. *Journal of Materials Research*, **16**, 2623–2633.

Výravský J. (2014) *Monazite, Xenotime and Zircon from Pegmatites in Dolní Bory*. Faculty of Science, Masaryk University Department of Geological Sciences, Brno, 81 pp.

Warr L.N. (2021) IMA-CNMNC approved mineral symbols. *Mineralogical Magazine*, **85**, 291–320.

https://doi.org/10.1180/mgm.2023.37 Published online by Cambridge University Press